Impregnation of KOAc on PdAu/SiO_2 causes Pd-acetate formation and metal restructuring

Hunter P. Jacobs,[a,‡] Welman C. Elias,[a,‡] Kimberly N. Heck,[a] David P. Dean,[b] Justin J. Dodson,[c] Wenqing Zhang,[a] Jacob H. Arredondo,[a] Christian J. Breckner,[b] Kiheon Hong,[d] Christopher R. Botello,[a] Laiyuan Chen,[c] Sean G. Mueller,[c] Steven R. Alexander,[c] Jeffrey T. Miller,[b] and Michael S. Wong[a,d,e,f]

[a]Department of Chemical and Biomolecular Engineering, Rice University, Houston, TX, 6100 Main Street, Houston, Texas 77005, USA
[b]Davidson School of Chemical Engineering, Purdue University, 480 Stadium Mall Drive, West Lafayette, Indiana 47907, USA
[c]Celanese Corporation, 9502 Bayport Blvd., Pasadena, TX 77507, USA
[d]Department of Civil and Environmental Engineering, Rice University, USA
[e]Department of Materials Science and NanoEngineering, Rice University, USA
[f]Department of Chemistry, Rice University, USA

[‡]*These authors contributed equally to the manuscript.*

[†]*Electronic supplementary information (ESI) available.*

***Corresponding author:* mswong@rice.edu**

Abstract:

Potassium-promoted, oxide-supported PdAu is catalytically active for the gas-phase acetoxylation of ethylene to form vinyl acetate monomer (VAM), in which the potassium improves long-term activity and VAM selectivity. The alkali metal is incorporated into the catalyst via wet impregnation of its salt solution, and it is generally assumed that this common catalyst preparation step has no effect on catalyst structure. However, in this work, we report evidence to the contrary. We synthesized a silica-supported PdAu ($PdAu/SiO_2$, 8 wt% Pd, 4 wt% Au) model catalyst containing Pd-rich PdAu alloy and pure Au phases. Impregnation with potassium acetate (KOAc) aqueous solution and subsequent drying did not cause XRD-detectible changes to the bimetal structure. However, DRIFTS indicated the presence of $Pd_3(OAc)_6$ species, which is correlated to up to 2% Pd loss after washing of the dried KOAc-promoted $PdAu/SiO_2$. Carrying out the impregnation step with an AcOH-only solution and subsequent drying caused significant enlargement of the pure Au grain size and generated a smaller amount of $Pd_3(OAc)_6$. During co-impregnation of AcOH and KOAc, grain sizes were enlarged slightly, and substantial amounts of $K_2Pd_2(OAc)_6$ and $Pd_3(OAc)_6$ were detected by DRIFTS and correlated to up to 32% Pd loss after washing. Synchrotron XAS analysis showed that approximately half the Pd atoms were oxidized, corroborating the presence of the Pd-acetate species. These results indicate wet-impregnation-induced metal leaching can occur, and can be substantial during catalyst preparation.

1. Introduction

Since the early 1900s, industrial vinyl acetate monomer (VAM) production has been a major contributor for the manufacture of products (*e.g.* paints, adhesives, and plastics) derived from polyvinyl acetate, polyvinyl alcohol, ethylene-vinyl acetate copolymer, ethylene-vinyl alcohol copolymer, and other polymers.[1,2] In the 1960s, Moiseev and Smidt[3] reported the liquid-phase acetoxylation of ethylene with acetic acid (AcOH) to produce VAM using a Pd^{2+} salt (typically $Pd(OAc)_2$ or $PdCl_2$) as catalyst and $CuCl_2$ as co-catalyst.[4,5] During the late 1960s and 1970s, an alternative industrial process was developed by the Hoechst and Bayer companies, which involved the heterogeneous gas-phase version of this reaction. It is the main process used to this date, due to increased selectivity to VAM as well as the avoidance of chloride salts which can lead to reactor corrosion.[6]

The typical catalyst is a PdAu composition supported on silica- and alumina-based supports and promoted with alkali salts, namely potassium acetate (KOAc).[6–13] PdAu alloys have enhanced catalytic properties in relation to monometallic Pd, not only for industrial-scale VAM synthesis,[8] but also for H_2O_2 formation,[14–16] glycerol selective oxidation,[17,18] and other reactions.[19,20] The enhancement has been attributed to both to electronic[21–23] and ensemble effects.[24–26] Once alloyed with Au, Pd loses *s*- and *p*-electrons to Au and gains *d*-electrons, shifting its *d*-band center away from its Fermi level (E_f).[21] This leads to weaker interaction between Pd sites and adsorbates. In VAM synthesis, Au is able to support isolated Pd surface atoms, and pairs of such atoms appropriately spaced apart have been implicated as the ideal active site.[26]

The addition of alkali promoters (*e.g.* KOAc) has been shown to profoundly enhance activity and selectivity to VAM for PdAu catalysts while also suppressing catalyst deactivation.[9] This has been attributed to the electronic influence of alkali metals on Pd. Hybridization of the alkali metal's *s*- and *p*-bands transfers electrons to Pd, lowering its *d*-band and, thereby, altering adsorption energies for acetate and ethylene.[27,28] It has also been claimed that KOAc suppresses ethylene combustion by reacting with AcOH to form $KH(OAc)_2$.[29,30] Evidence for the presence of a physisorbed AcOH multilayer over the catalyst surface under reaction conditions has been reported.[5,6,31,32] Pd is known to be soluble in these AcOH multilayer films as either trimeric $Pd_3(OAc)_6$ or dimeric $Pd_2(OAc)_4$ species.[5] In the presence of alkali acetates (MOAc), Pd-acetates can take the form of dimeric $M_2Pd_2(OAc)_6$ or monomeric $M_2Pd(OAc)_4$,[33–35] which was shown to

form under reaction conditions by Lercher and coworkers in the observed PdAu metal restructuring.[9–11]

In the preparation of PdAu catalysts for vinyl acetate synthesis, alkali acetate promoters are incorporated via wet impregnation. However, the catalyst structure should not be considered immutable during this preparation step. Given its affinity to form Pd-acetates in liquid environments as well as under gas-phase VAM reaction conditions,[5,9–11] we speculate that Pd-acetates could form during KOAc impregnation, leading to Pd leaching and metal restructuring prior to catalytic reaction, which has not been considered by prior reports. In this work, we synthesized SiO_2-supported PdAu catalysts and impregnated them with KOAc aqueous solution. We additionally carried out wet impregnation using a AcOH solution and KOAc/AcOH solution to understand the impact of AcOH on Pd-acetate species formation. We analyzed structural modifications through XRD, XPS, and XAS, surface species formation through DRIFTS, and metal leaching after catalyst washing via ICP-OES. Collectively, our findings emphasize that common wet impregnations methods may alter catalyst structure and composition prior to introduction to the reaction environment.

2. Experimental

2.1 Materials

Sodium tetrachloropalladate (Na_2PdCl_4, ≥98%), gold chloride trihydrate ($HAuCl_4 \cdot 3H_2O$, ≥99.9%), silica gel (SiO_2, 40 – 63 μm particle size, ≥480 m^2/g surface area), sodium carbonate (Na_2CO_3, ≥99%), and potassium acetate (KOAc, ≥99%) were purchased from Sigma-Aldrich. Glacial acetic acid (AcOH, ≥99.7% w/w) was purchased from Fisher Scientific. Nitrogen (N_2, 99.999%), hydrogen (H_2, 99.999%), and 10% oxygen (10% O_2/bal. He) gases were purchased from Airgas. All experiments were conducted using deionized (DI) water (≥18 MΩ·cm, Thermo Scientific MicroPure).

2.2 Synthesis of SiO_2-supported PdAu Nanoparticles

PdAu nanoparticles supported on silica (SiO_2) were prepared with a Pd:Au weight ratio of 2 by methods previously reported in the literature.[36] Briefly, Na_2PdCl_4 and $HAuCl_4$ metal precursors were added to SiO_2 powder by incipient wetness impregnation. After drying overnight at 80 °C, the powder was mixed with 0.4 M Na_2CO_3 solution (25 mL per 5 g of sample), followed by drying

overnight at 80 °C. The sample was repeatedly washed with DI water (~1 L water per 5 g of sample) and dried once more overnight at 80 °C. Samples were placed in a furnace with a tubular quartz cell and reduced under flowing H_2 gas atmosphere at 150 °C for 1 hr. Target metal loadings of 8 wt% Pd and 4 wt% Au were confirmed by ICP-OES.

The as-synthesized PdAu/SiO_2 sample was then loaded with various amounts of KOAc by incipient wetness impregnation to achieve K loadings of 0, 5, or 10 wt% K. The KOAc solution also contained varying concentrations of AcOH (water-only, AcOH-only, and 50% v/v AcOH in water). The treated samples were then dried at 80 °C overnight.

After all characterization was performed, 250 mg of each sample was washed and vacuum-filtered with 45 mL of DI water. The filtrate was collected and analyzed by ICP-OES to quantify Pd, Au, and K metals recovered in the filtrate.

2.3 XRD Characterization

X-ray powder diffraction (XRD) profiles were collected using a Philips X'Pert Pro diffractometer equipped with a Cu Kα radiation source (1.540598 Å) generated at 45 kV and 40 mA. XRD analysis was conducted in a 2θ range of 30 – 70° with a step size of 0.0050° s^{-1}. The XRD (111) peaks for Pd, Au, and PdAu were analyzed using OriginLab by deconvoluting the 111 planes with a Voigt function. The obtained XRD maximum peak intensity and FWHM were then used to calculate the phase composition and grain size by applying Vegard's[37] (Eqn. 1) and Scherrer's[38] (Eqn. 2) equations, respectively:

$$a_{Pd_xAu_{(1-x)}} = xa_{Pd} + (1-x)a_{Au} \quad (1)$$

$$d = \frac{K\lambda}{\beta cos\theta} \quad (2)$$

where $a_{Pd_xAu_{(1-x)}}$ is the lattice parameter of the PdAu alloy, a_{Pd} and a_{Au} are the lattice parameters of the pure constituents, x is the Pd mole fraction, d is the mean grain size, K is the proportionality constant, λ is the X-ray wavelength, β is the peak full width at half maximum (FWHM) in radians, and θ is the Bragg angle in radians.

2.4 XPS Characterization

X-ray photoelectron spectroscopy (XPS) was performed on a PHI Quantera SXM (ULVAC-PHI. Inc) spectrometer equipped with an Al monochromator. $PdAu/SiO_2$ samples were analyzed under UHV conditions at the Pd 3d and Au 4f core levels. The Si 2p core level was also measured and used to normalize all binding energy values to Si 2p = 103.5 eV for pure silica.[39] XPS peak fittings and surface metal compositions were calculated using Multipak (ULVAC-PHI. Inc) XPS fitting software.

2.5 DRIFTS Characterization

Diffuse reflectance infrared Fourier transform spectroscopy (DRIFTS) experiments were performed on a Thermo Scientific Nicolet iS10 FTIR spectrometer equipped with a liquid-N_2-cooled HgCdTe (MCT) detector. A high-temperature reaction chamber equipped with ZnSe windows, mounted on a Praying Mantis diffuse reflectance accessory (Harrick Scientific), was used for *in situ* gas-phase analysis of $PdAu/SiO_2$ samples at 25 °C under N_2 atmosphere at 10 torr total pressure. Temperature was monitored by positioning a type-K thermocouple in the sample cup and controlled using an ATK temperature controller (Harrick Scientific). The as-synthesized $PdAu/SiO_2$ sample was used to collect a background spectrum for all samples. All spectra are reported in Kubelka-Munk units by averaging 128 scans at 4 cm^{-1} resolution. Peak locations and integrated intensities were determined for each vibrational mode by fitting with a Voigt function in OriginLab.

2.6 XAS Characterization

In situ X-ray absorption spectroscopy (XAS) experiments were performed at the 10-ID beamline[40] at the Advanced Photon Source (APS), Argonne National Laboratory (ANL), at the Au L_{III} edge (11.919 keV) and the Pd K edge (24.350 keV) in transmission mode with an energy resolution of 0.5 eV and edge energy precision greater than 0.1 eV. All samples were ground into a fine powder, pressed into a six-shooter sample holder, and placed in a quartz sample cell with X-ray transparent Kapton end caps. The end caps seal the sample cell and permit the connection of gases to flow through the cell. Each scan was accompanied by simultaneous acquisition of either a Au or Pd foil absorption spectra obtained via a third ion chamber used for energy calibration. All $PdAu/SiO_2$ samples were scanned at both the Au L_{III} and Pd K edge under flowing 10% O_2/He at 30 °C.

XAS data was fit using winXAS 3.1 software.[41] X-ray absorption near edge structure (XANES) was used to determine the edge energy of each sample at the Pd and Au edges. Least-squares regression fits of the k^2-weighted Fourier transform data from 2.4 to 12 Å^{-1} for Pd and 2.6 to 11 Å^{-1} for Au in *k*-space were used to obtain the extended X-ray absorption fine structure (EXAFS) coordination parameters. The first shell was used to fit all spectra. All samples were fit using theoretical scattering paths using FEFF6.[42] An S_0^2 value of 0.79 at a fixed coordination number of 12 and bond distance of 2.75 Å was determined using the Pd foil, and an S_0^2 value of 0.83 at a fixed coordination number of 12 and bond distance of 2.88 Å was determined using the Au foil.

2.7 Multivariate Analysis

Multivariate analysis was performed using a three-level full factorial experimental design with AcOH vol% and K wt% as the two factors (*i.e.* 3^2 full factorial experimental design). Each factor had a low level (-1), center level (0), and high level (+1), which are outlined in Table 1. Triplicate samples were synthesized at the level-(0,0) center point, leading to 11 total samples.

Table 1. Factors and levels for 3^2 full factorial experimental design

Factor	**Level**		
	-1	**0**	**+1**
AcOH (vol%)	0	50	100
K (wt%)	0	5	10

Response variables describing metal structure and surface species were selected from XRD, XPS, XAS, DRIFTS, and ICP-OES data. Least-squares linear regression fits of the responses were calculated using Minitab software to generate response surface plots considering the effects of AcOH vol% and K wt%. The linear regression model is described by the following equation:

$$y(x_1, x_2) = C_0 + C_1x_1 + C_2x_2 + C_{11}{x_1}^2 + C_{22}{x_2}^2 + C_{12}x_1x_2 \quad (3)$$

where y is the estimated response as a function of the factors, x_i is the *i*th factor (*i.e.* AcOH vol% and K wt%), C_0 is the constant coefficient, C_i is the linear coefficient of the *i*th factor, C_{ii} is the quadratic coefficient of the *i*th factor, and C_{12} is the interaction coefficient.

Analysis of variance (ANOVA) tests were performed to evaluate which effects in the regression model had statistically significant (95% confidence level, α = 0.05) contributions for each response variable. The results are presented as Pareto charts of the standardized effects generated by Minitab software. Further details on the statistical analysis methods are provided in the Supporting Information.

3. Results and Discussion

3.1 Effects of KOAc Impregnation on PdAu Nanostructure

The bulk Pd_xAu_y alloy composition in the as-synthesized $PdAu/SiO_2$ sample was determined by analyzing the (111) peaks in its XRD pattern (in the 2θ region from 36° to 42°, Figure 1a). The as-synthesized $PdAu/SiO_2$ consisted of two distinct phases: one Au-rich phase, and one Pd-rich phase. Using the pure Au(111) (gold line) and Pd(111) (blue line) peaks at 38.2° and 40.2°, respectively, as references[43,44] and applying Vegard's law, the two phases are calculated to be a pure Au phase and a Pd-rich $Pd_{75}Au_{25}$ alloy phase.

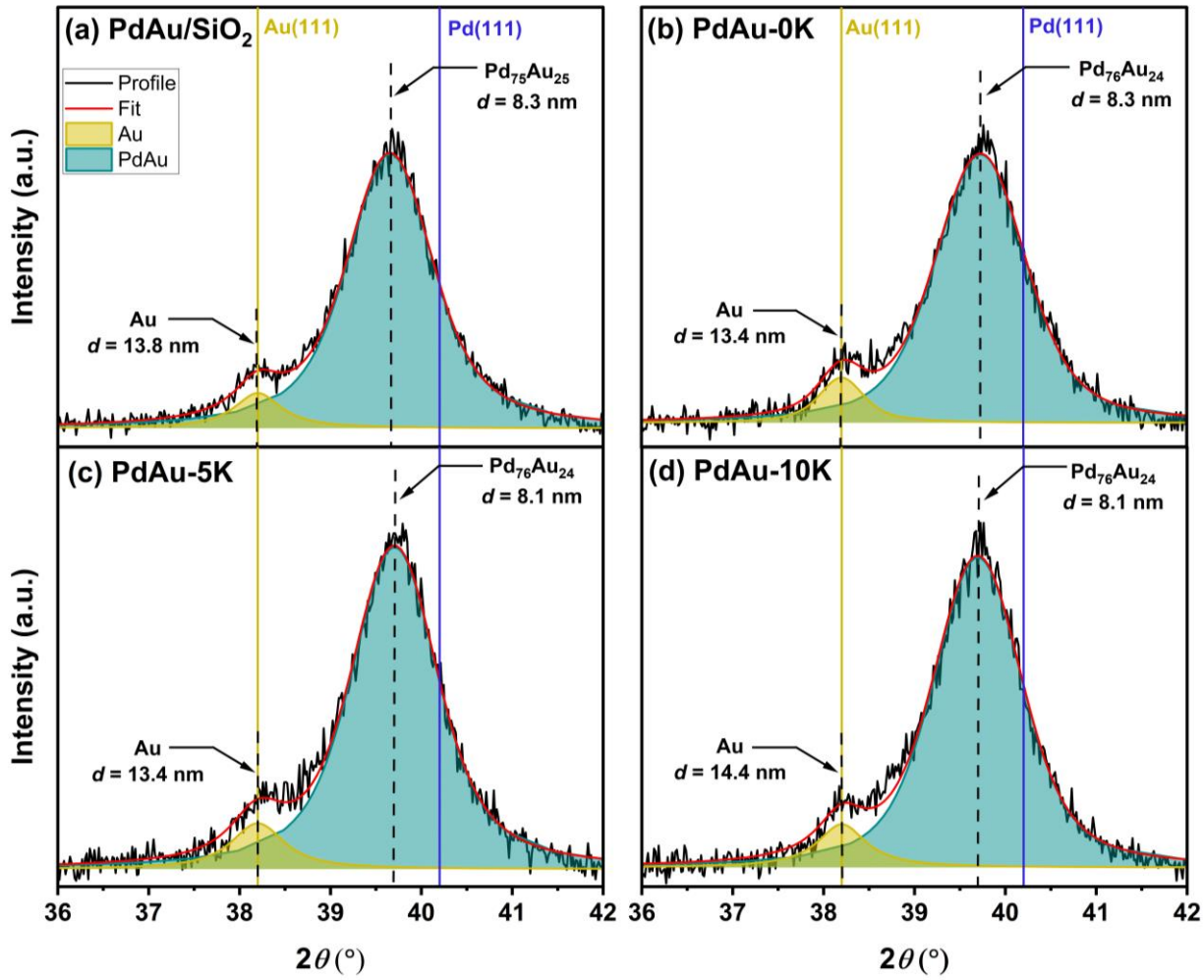

Figure 1. XRD profiles of the (a) as-synthesized PdAu/SiO_2 (8 wt% Pd, 4 wt% Au), (b) water-treated PdAu/SiO_2 (PdAu-0K), and KOAc-impregnated PdAu/SiO_2 containing (c) 5 wt% K (PdAu-5K) and (d) 10 wt% K (PdAu-10K). Blue line represents Pd(111) reference, and the gold line represents Au(111) reference. Green curve represents the Pd-rich PdAu alloy phase, and the gold curve represents pure Au phase.

From Scherrer's equation, the grain sizes (*d*) of the pure Au phase and $Pd_{75}Au_{25}$ phase were 8.3 and 13.8 nm, respectively (Table 2). Since particles with grain sizes smaller than 3 nm and metal acetates are not detectible via XRD using a standard Cu Kα X-ray source, atoms within these domains are considered "XRD-invisible." Utilizing the relative amounts of each phase and assuming all Au atoms are observed in the XRD pattern, we estimated that 45% of Pd atoms are XRD-invisible on the as-synthesized PdAu/SiO_2 sample.

Table 2. Phase compositions, grain sizes, and Pd:Au surface ratio of as-synthesized, water-treated, and KOAc-treated $PdAu/SiO_2$.

Sample	Phase composition[a] (at%)	Grain size[b] (nm)	Pd:Au surface ratio[c] (at%)
$PdAu/SiO_2$	Au	13.8	80:20
	$Pd_{75}Au_{25}$	8.3	
PdAu-0K	Au	13.4	80:20
	$Pd_{76}Au_{24}$	8.3	
PdAu-5K	Au	13.4	79:21
	$Pd_{76}Au_{24}$	8.1	
PdAu-10K	Au	14.4	77:23
	$Pd_{76}Au_{24}$	8.1	

[a]Calculated from XRD data using Vegard's equation.
[b]Calculated from XRD data using Scherrer's equation.
[c]Calculated from XPS data at Pd 3d and Au 4f core levels.

XRD analysis was performed after wet impregnation of various loadings of KOAc (water-only, and 5 and 10 wt% K) on the $PdAu/SiO_2$ samples (herein labeled "PdAu-0K," "PdAu-5K," and "PdAu-10K," respectively) in order to investigate any changes to the bulk PdAu nanostructure. No significant changes to the bulk PdAu structure were observed due to KOAc loading as detected by XRD (Figure 1b-d). All samples maintained a pure Au phase and a Pd-rich PdAu alloy phase containing 76 at% Pd, consistent with the as-synthesized $PdAu/SiO_2$ (Table 2). Grain sizes of the pure Au and PdAu alloy phases were calculated to be 8.1 – 8.3 nm and 13.3 – 14.4 nm, respectively (Table 2). The amount of XRD-invisible Pd was also calculated to be 42 – 44%. The wet impregnation procedure (with and without KOAc) had negligible (within ±10% error) effect on the metal crystal structure.

XPS was performed at the Pd 3d and Au 4f core levels in order to confirm complete reduction of Pd and Au on the as-synthesized $PdAu/SiO_2$. A single asymmetric peak was observed at 334.6 eV in the Pd $3d_{5/2}$ region coupled with a Pd $3d_{3/2}$ peak located 5.3 eV higher due spin-orbit splitting (Figure 2a). Likewise, a single asymmetric peak was also observed at 83.0 eV in the Au $4f_{7/2}$ region coupled with a Au $4f_{5/2}$ peak located 3.7 eV higher (Figure 2b). These peaks are characteristic of reduced Pd^0 and Au^0 found in PdAu alloys,[45] confirming complete reduction of both Pd and Au.

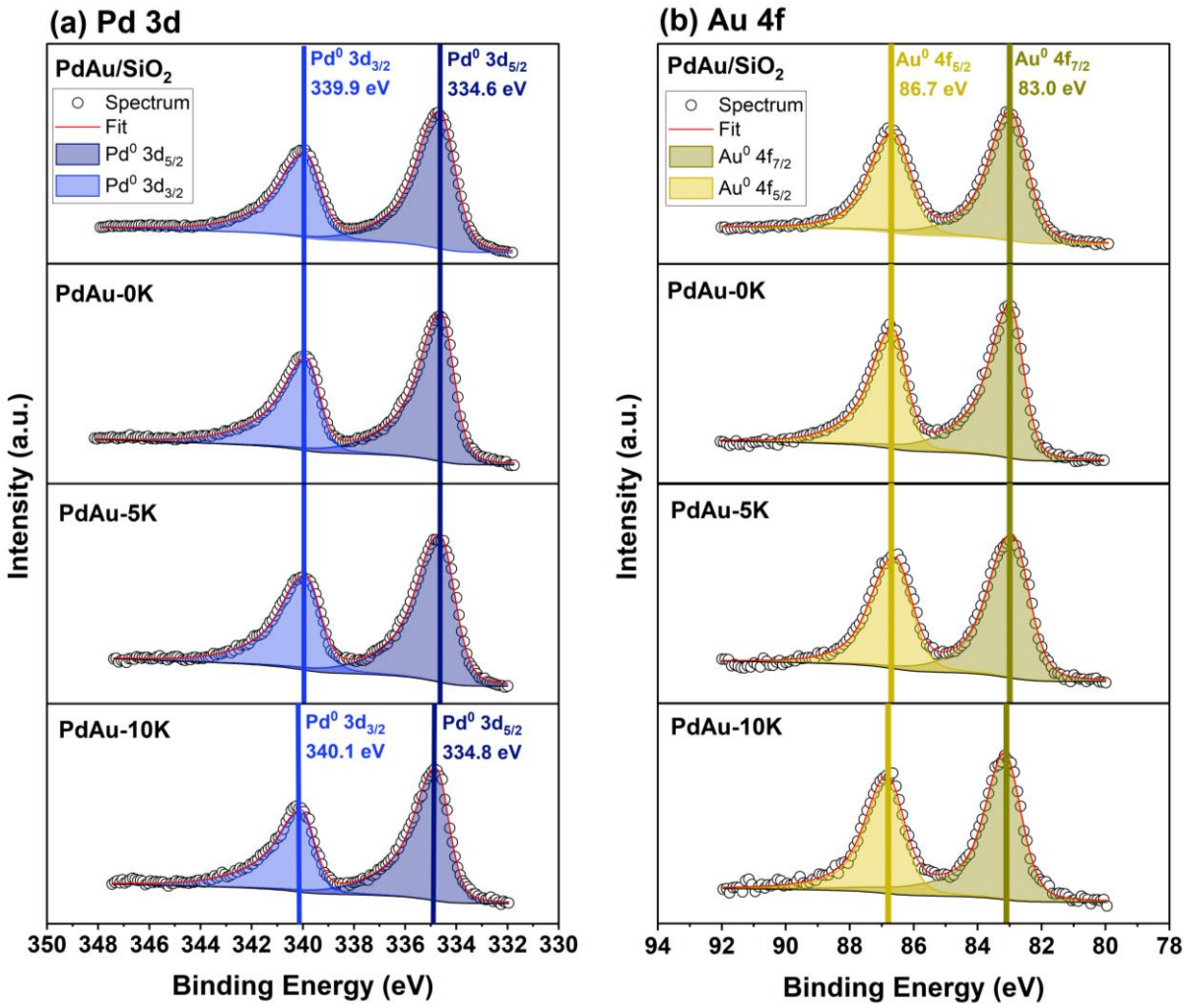

Figure 2. XPS spectra at the (a) Pd 3d and (b) Au 4f core levels of the as-synthesized PdAu/SiO_2 (8 wt% Pd, 4 wt% Au), water-treated PdAu/SiO_2 (PdAu-0K), and KOAc-impregnated PdAu/SiO_2 containing 5 wt% K (PdAu-5K) and 10 wt% K (PdAu-10K). BE values are ±0.1 eV.

Both the observed Pd $3d_{5/2}$ and Au $4f_{7/2}$ peaks are shifted to lower binding energies compared to expected binding energies of monometallic Pd^0 (Pd $3d_{5/2}$ = 335.0 eV) and Au^0 (Au $4f_{7/2}$ = 84.0 eV),[46] suggesting greater electron density at those respective core levels. These observations are consistent with findings from Lee et al. who suggested Pd gains *d*-electrons from Au, while Au gains overall electron density via *s*- and *p*-electron donation from Pd.[45] The Pd:Au surface ratio was calculated to be 80:20 at% (Table 2), consistent with the expected bulk ratio for a PdAu sample with 8 wt% Pd and 4 wt% Au.

XPS analysis was also performed on the PdAu-0K, PdAu-5K, and PdAu-10K samples in order to investigate changes in metal oxidation states caused by KOAc wet impregnation. No

additional peaks were observed after addition of KOAc to the as-synthesized PdAu/SiO_2 sample (Figure 2), indicating both Pd and Au remained reduced. No significant binding energy shifts or changes to Pd:Au surface ratio were observed for the PdAu-0K and PdAu-5K samples (Figure 2, Table 2). However, a slight binding energy shift of the Pd $3d_{5/2}$ core level to 334.8 eV occurred on the PdAu-10K sample with high KOAc loading (Figure 2a), indicating loss of electron density on the metal surface. We speculate this is due to acetate adsorption where some *d*-electrons of surface Pd would be donated for Pd-OAc bond formation. While interactions between surface Pd and potassium cannot be completely discounted, their contributions would instead cause the Pd 3d binding energy to shift to lower values since alkali metals are reported to donate electrons to Pd and other transition metals through hybridization of their *s*- and *p*-orbitals.[27,28,47–50] The observed binding energy shift also corresponded to a slight decrease in Pd content on the surface when compared to the samples without KOAc or with lower concentration (*i.e.* Pd:Au surface ratio = 77:23 at% *vs* 80:20 at% for PdAu-10K and PdAu-0K, respectively, Table 2).

3.2 DRIFTS Analysis of KOAc-treated PdAu/SiO_2

DRIFTS was performed on the water-treated and KOAc-impregnated samples in order to detect surface acetate species. Figure 3 shows DRIFTS spectra and peak deconvolution of the PdAu-0K, PdAu-5K, and PdAu-10K samples from 2000 – 1100 cm^{-1}, highlighting species in the acetate region.

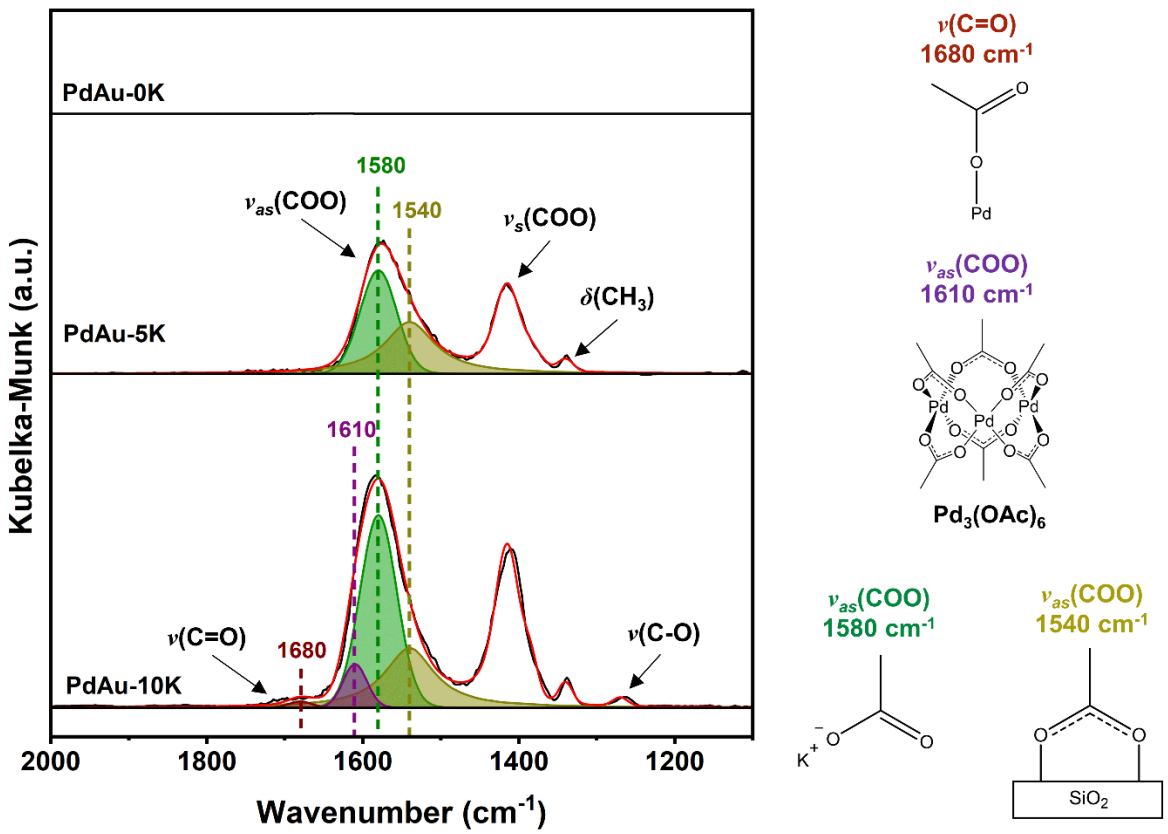

Figure 3. Deconvoluted DRIFTS spectra in the 2000 – 1100 cm^{-1} acetate region of the water-treated $PdAu/SiO_2$ (PdAu-0K) and KOAc-impregnated $PdAu/SiO_2$ with 5 wt% K (PdAu-5K) and 10 wt% K (PdAu-10K) loadings. ν(C=O) peaks are located between 1800 – 1670 cm^{-1}. ν_{as}(COO) peaks are located between 1670 – 1500 cm^{-1}. ν_s(COO) peaks are located between 1450 – 1390 cm^{-1}. $\delta(CH_3)$ peaks are located between 1390 – 1300 cm^{-1}. ν(C-O) peaks are located between 1300 – 1250 cm^{-1}. As-synthesized $PdAu/SiO_2$ was used as background for all samples.

Peak deconvolution of the DRIFTS spectra (Figure 3) reveal many peaks in the ν(C=O) and ν_{as}(COO) regions characteristic of distinct acetate species. The PdAu-0K sample showed no peaks in the acetate region, as expected. The most prominent species present on both PdAu-5K and PdAu-10K is located at 1580 cm^{-1} and attributed to ionic acetate (*i.e.* KOAc).[9] A second species present on both samples located at 1540 cm^{-1} is likely acetate adsorbed on SiO_2 in a bridging mode.[51,52] This species is also associated with a negative peak at 3750 cm^{-1} attributed to hydroxyl stretching (ν(OH)) of isolated silanols on the SiO_2 surface,[53] indicating conversion of surface silanols to either silyl acetates or alkali silanolates (Figure S1a). Interestingly, the PdAu-10K sample containing the highest KOAc loading contains two additional peaks at 1680 and 1610

298 cm^{-1}. We attribute the peak at 1680 cm^{-1} to be the ν(C=O) vibration of acetate adsorbed on surface
299 Pd in a terminal, monodentate mode, which pairs with a ν(C-O) peak at 1270 cm^{-1}.[54] The peak at
300 1610 cm^{-1} is characteristic of the ν_{as}(COO) vibration of $Pd_3(OAc)_6$ trimers.[9] The presence of these
301 two species at high KOAc loading indicates that KOAc directly interacts with surface Pd to form
302 either surface Pd-acetates or molecular $Pd_3(OAc)_6$ trimers. Additional peaks located between 1450
303 – 1300 cm^{-1} are attributed to symmetric carboxylate stretching (ν_s(COO)) and CH_3 deformation
304 ($\delta(CH_3)$) vibrational modes characteristic of acetate.

305 Since Kubelka-Munk units have previously been reported to scale linearly with surface
306 species concentration,[55] integrated peak intensities are used to quantify relative amounts of acetate
307 species in the absence of known IR extinction coefficients. Figure S2a provides the quantification
308 of concentrations for different acetate species based on the integrated intensities of the ν(C=O) and
309 ν_{as}(COO) vibrational modes versus K wt%. The PdAu-0K sample shows no intensity for any
310 acetate species, as expected. The ionic acetate species (*i.e.* KOAc) roughly doubles as KOAc
311 loading also doubles, showing a linear trend. The PdAu-5K sample initially contained similar
312 quantities of ionic acetate and silyl acetate; however, the silyl acetate quantity only marginally
313 increased when 10 wt% K was added in the PdAu-10K sample, suggesting that the addition of 5
314 wt% K is sufficient to convert available surface silanols to silyl acetates. Figure S2a also indicates
315 small amounts of surface Pd-acetates and $Pd_3(OAc)_6$ trimers were present on the PdAu-10K
316 sample.

317 After DRIFTS identification of the formation of Pd-acetate species at high KOAc loadings,
318 we washed and filtered the samples with water. We then analyzed the collected filtrate by ICP-
319 OES to quantify recovered metals (Pd, Au, and K). The amount of each metal that was recovered
320 in the filtrate for each sample is presented in Table 3 as a percentage of initial metal loading (initial
321 loadings of Pd = 8 wt%, Au = 4 wt%, and K = 0, 5, or 10 wt%).

322

323 **Table 3.** ICP-OES analysis of metals recovered in filtrate after washing KOAc-treated samples
324 with water.

Sample	Pd recovered (% of initial)	Au recovered (% of initial)	K recovered (% of initial)
PdAu-0K	0.7	0	-
PdAu-5K	1.7	0	90
PdAu-10K	2.1	0	95

325

For all samples, no Au was detected in the filtrate, indicating no Au leached from the samples. We were also able to achieve >90% recovery of K for the PdAu-5K and PdAu-10K samples, confirming initial loadings of 5 wt% and 10 wt% K, respectively. Small amounts of Pd were detected in the filtrate ranging from 0.7 – 2.1% of initial Pd loading. Interestingly, while the total Pd amount leached was relatively small, there is a noticeable trend that increasing KOAc loading led to greater Pd loss in the filtrate (Table 3). This Pd loss is due to Pd-acetate species leached out during the wash, which was further confirmed by DRIFTS analysis of the washed samples via the absence of IR peaks typical of KOAc and Pd-acetate species (Figure S3a).

3.3 Effects of Impregnating with AcOH and AcOH/KOAc Solutions on PdAu Nanostructure

In the previous section, we showed that high KOAc loadings led to the formation of Pd-acetate species. To further explore the formation of Pd-acetate species and metal nanoparticle restructuring, we replaced aqueous KOAc wet impregnation solutions with glacial AcOH as a possible acetate source to prepare one sample labeled "PdAu-0K-100AA." No noticeable changes in phase composition were observed, *i.e.*, the metals retained the pure Au phase and a Pd-rich PdAu alloy phase of 75 at% Pd (Figure 4a). The grain sizes of the pure Au and Pd-rich phases were calculated to be 20.2 nm and 8.6 nm, respectively (Table 4). Whereas the PdAu grain size only slightly grew compared to the as-synthesized PdAu/SiO_2, the Au grain size enlargement was more pronounced. This suggests Au nanoparticles tend to aggregate under acidic conditions, possibly due to surface charge effects on the support.[56–58] Approximately 45% of Pd atoms were "XRD-invisible."

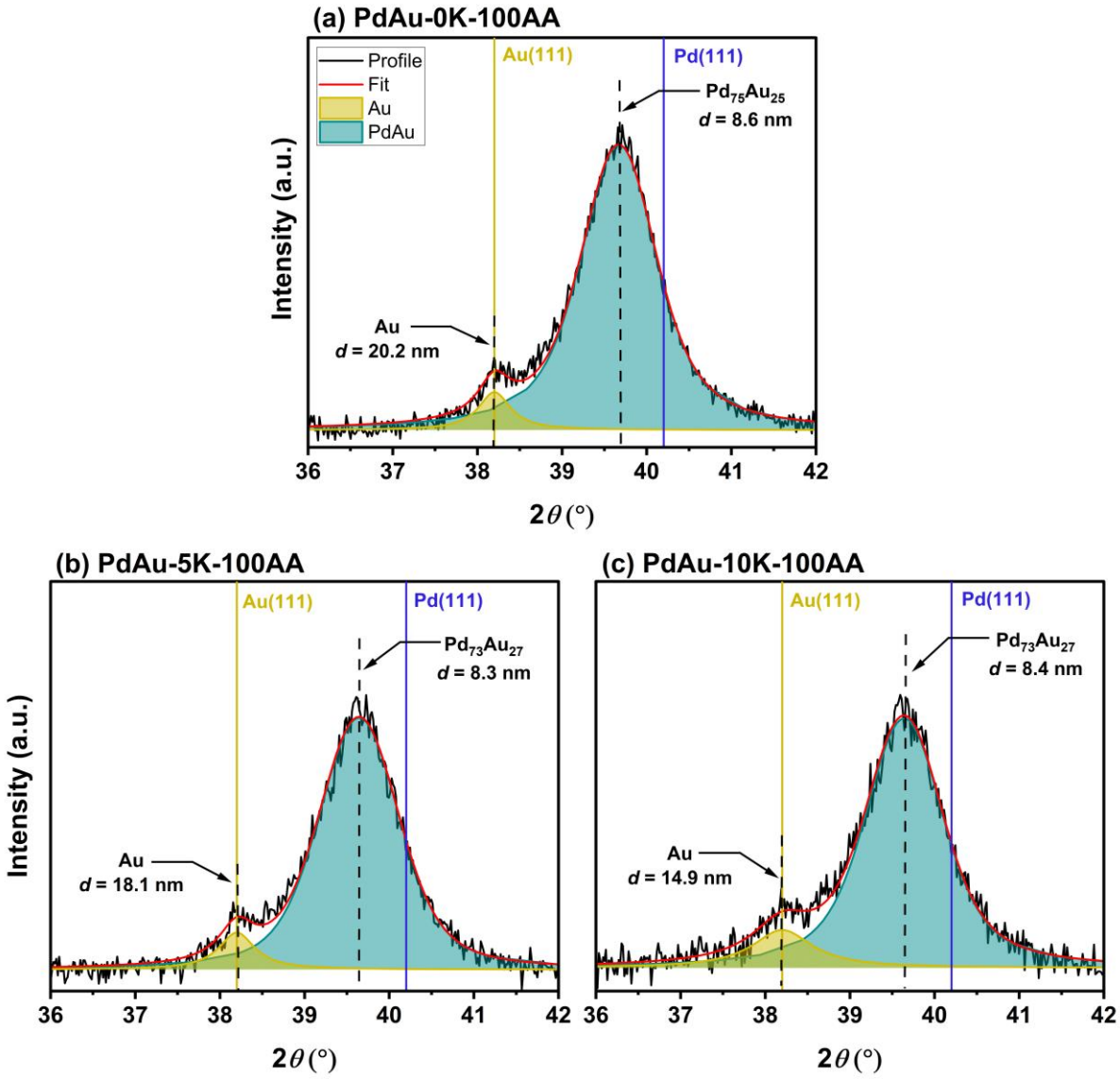

Figure 4. XRD profiles of the (a) PdAu/SiO_2 treated in glacial AcOH (PdAu-0K-100AA) and KOAc-impregnated PdAu/SiO_2 treated in glacial AcOH containing (b) 5 wt% K (PdAu-5K-100AA) and (c) 10 wt% K (PdAu-10K-100AA). Blue line represents Pd(111) reference, and the gold line represents Au(111) reference. Green curve represents the Pd-rich PdAu alloy phase, and the gold curve represents pure Au phase.

Table 4. Phase compositions, grain sizes, and Pd:Au surface ratio of AcOH-treated and AcOH/KOAc-treated PdAu/SiO_2.

Sample	Phase composition[a] (at%)	Grain size[b] (nm)	Pd:Au surface ratio[c] (at%)
PdAu-0K-100AA	Au	20.2	79:21
	$Pd_{75}Au_{25}$	8.6	
PdAu-5K-100AA	Au	18.1	76:24

	$Pd_{73}Au_{27}$	8.3	
PdAu-10K-100AA	Au	14.9	68:32
	$Pd_{73}Au_{27}$	8.4	

[a]Calculated from XRD data using Vegard's equation.
[b]Calculated from XRD data using Scherrer's equation.
[c]Calculated from XPS data at Pd 3d and Au 4f core levels.

To explore the effect of wet impregnation using combinations of AcOH and KOAc, we prepared two samples, labeled "PdAu-5K-100AA" and "PdAu-10K-100AA," containing 5 wt% and 10 wt% K dissolved in glacial AcOH, respectively. Their phase composition and PdAu alloy grain sizes were essentially the same as those of "PdAu-0K-100AA," however, the Au grain size decreased considerably as K content increased (Figure 4b-c, Table 4). We hypothesize the addition of KOAc neutralized AcOH creating a buffer solution and, thus, inhibited Au nanoparticle growth. The amount of "XRD-invisible" Pd was calculated to be 48 – 50%.

XPS analysis was also performed on the PdAu-0K-100AA, PdAu-5K-100AA, and PdAu-10K-100AA samples. Pd and Au remained reduced as no additional peaks were detected (Figure 5). A binding energy shift of the Pd $3d_{5/2}$ core level to 335.0 eV on the PdAu-5K-100AA and PdAu-10K-100AA samples compared to the as-synthesized PdAu (Pd $3d_{5/2}$ = 334.6 eV) suggests further interaction of acetate with surface Pd (Figure 5a). This also led to a decrease in surface Pd content to 68 at% in the PdAu-10-100AA sample (Table 4). Interestingly, the PdAu-0K-100AA sample without KOAc did not show such a shift, indicating that acetate, rather than acetic acid, interacts with surface Pd.

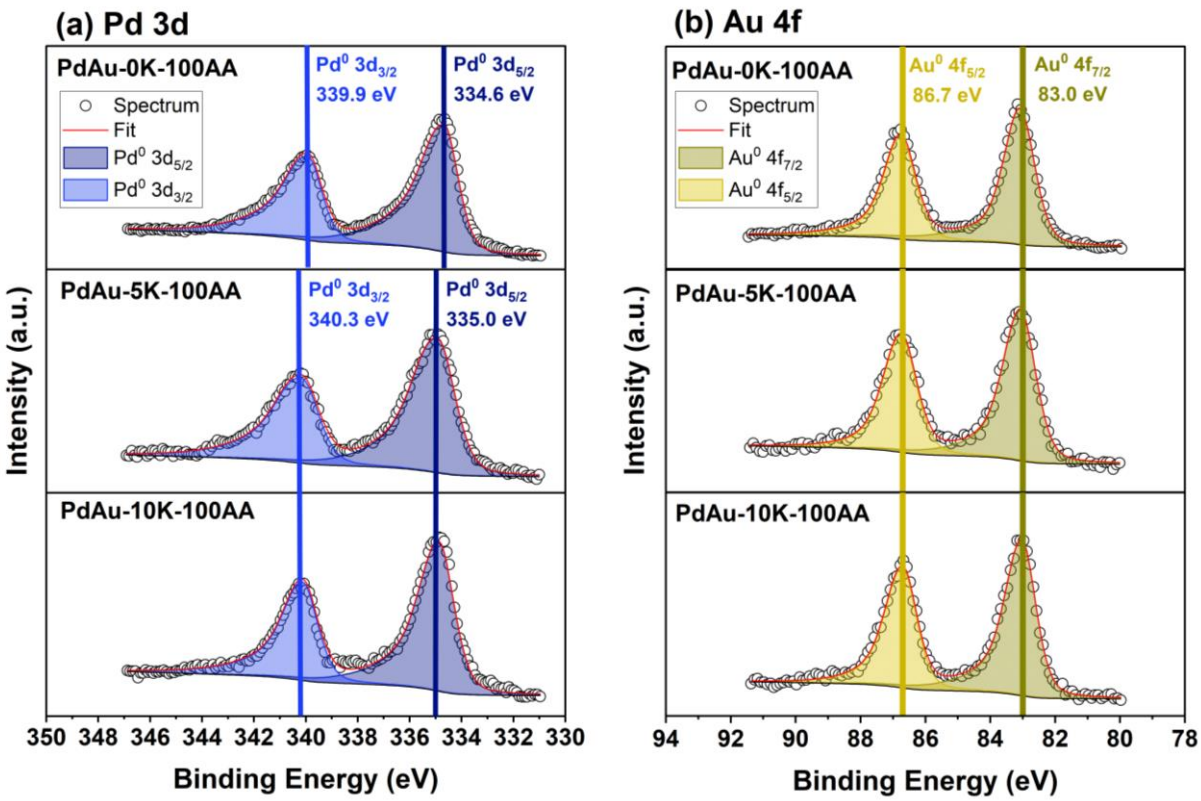

Figure 5. XPS spectra at the (a) Pd 3d and (b) Au 4f core levels of the PdAu/SiO_2 treated in AcOH (PdAu-0K-100AA) and KOAc-impregnated PdAu/SiO_2 treated in AcOH containing 5 wt% K (PdAu-5K-100AA) and 10 wt% K (PdAu-10K-100AA). BE values are ±0.1 eV.

3.4 DRIFTS Analysis of PdAu/SiO_2 treated with AcOH and AcOH/KOAc Solutions

DRIFTS was performed on the AcOH/KOAc-treated samples in order to detect surface acetate species. Figure 6 shows DRIFTS spectra and peak deconvolution of the PdAu-0K-100AA, PdAu-5K-100AA, and PdAu-5K-100AA samples in the acetate region from 2000 – 1100 cm^{-1}. Similar to the KOAc-treated samples, numerous carbonyl stretching (ν(C=O)) and asymmetric carboxylate stretching (ν_{as}(COO)) peaks associated with acetates are located between 1800 – 1500 cm^{-1} for the AcOH/KOAc-treated samples. As expected, a large ionic acetate (*i.e.* KOAc) peak located at 1580 cm^{-1} is present on the samples containing KOAc. The sample treated with only AcOH (PdAu-0K-100AA) also shows a small ionic acetate peak, likely in the form of NaOAc due to residual Na^+ remaining from the Na_2PdCl_4 precursor during synthesis. All samples show the bridged silyl acetate peak at 1540 cm^{-1}, paired with a negative ν(OH) peak at 3750 cm^{-1} (Figure S1b) attributed to conversion of isolated silanols to either silyl acetates or alkali silanolates. The ν(COO) peak of $Pd_3(OAc)_6$ trimers at 1610 cm^{-1} is also present for all samples. The samples containing KOAc

(PdAu-5K-100AA and PdAu-10K-100AA) show peaks at 1680 cm^{-1} indicating acetate adsorbed on surface Pd in a monodentate mode.

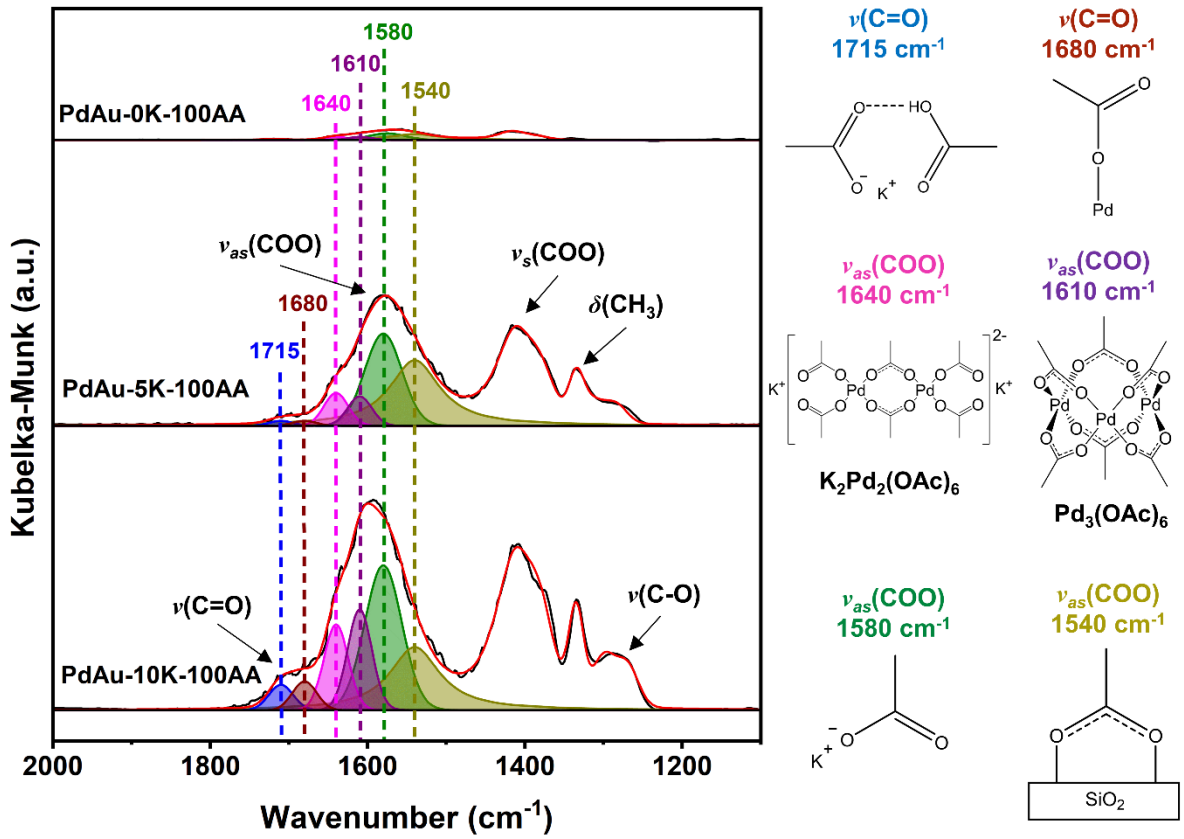

Figure 6. Deconvoluted DRIFTS spectra in the 2000 – 1100 cm^{-1} acetate region of the PdAu/SiO_2 treated in glacial AcOH (PdAu-0K-100AA) and KOAc-impregnated PdAu/SiO_2 treated in glacial AcOH containing 5 wt% K (PdAu-5K-100AA) and 10 wt% K (PdAu-10K-100AA). ν(C=O) peaks are located between 1800 – 1670 cm^{-1}. ν_{as}(COO) peaks are located between 1670 – 1500 cm^{-1}. ν_s(COO) peaks are located between 1450 – 1390 cm^{-1}. $\delta(CH_3)$ peaks are located between 1390 – 1300 cm^{-1}. ν(C-O) peaks are located between 1300 – 1250 cm^{-1}. As-synthesized PdAu/SiO_2 was used as background for all samples.

Interestingly, we observe two additional peaks not previously identified on the KOAc-treated samples in earlier sections located at 1715 cm^{-1} and 1640 cm^{-1}. The peak at 1715 cm^{-1} is likely attributed to the ν(C=O) vibration mode of $KH(OAc)_2$ since KOAc and AcOH are known to form a dimeric salt when in solution.[30] This is also paired with multiple ν(C-O) peaks present between 1300 – 1250 cm^{-1}. The peak at 1640 cm^{-1} falls between the terminal, monodentate Pd-

acetate peak at 1680 cm^{-1} and the bridging $Pd_3(OAc)_6$ trimer peak at 1610 cm^{-1}, suggesting this is a Pd-acetate species with a mixture of bridging and terminal acetates. We therefore attribute this peak at 1640 cm^{-1} to dimeric $K_2Pd_2(OAc)_6$, which is known to form in solutions of $Pd_3(OAc)_6$, KOAc, and AcOH.[5,9,34] Various ν_s(COO) and $\delta(CH_3)$ acetate peaks located between 1450 – 1300 cm^{-1} are also present on all samples.

Figure S2b provides a relative quantification of the concentration of different acetate species based on the integrated intensities of the ν(C=O) and ν_{as}(COO) vibrational modes as a function of added K. Although the AcOH-only-treated (PdAu-0K-100AA) sample shows small amounts of acetate species, it is clear that KOAc must also be present in order to produce acetate species in significant quantities. The ionic acetate species (*i.e.* KOAc) once again shows a linear correlation with KOAc loading. Generally, high amounts of KOAc lead to significant quantities of bridged silyl acetates. Figure S2b also indicates the large amount of surface Pd-acetates, $K_2Pd_2(OAc)_6$ dimers, and $Pd_3(OAc)_6$ trimers present on samples with high KOAc loading.

The three AcOH/KOAc-treated samples were washed with water and filtered in order to separate any water-soluble metals from the powder, and the collected filtrate was analyzed by ICP-OES to quantify recovered metals (Pd, Au, and K). The amount of each metal recovered in the filtrate for each sample is presented in Table 5 as a percentage of initial metal loading (initial loadings of Pd = 8 wt%, Au = 4 wt%, and K = 0, 5, or 10 wt%).

Table 5. ICP-OES analysis of metals recovered in filtrate after washing the AcOH-treated and AcOH/KOAc-treated samples with water.

Sample	Pd recovered (% of initial)	Au recovered (% of initial)	K recovered (% of initial)
PdAu-0K-100AA	7.4	0	-
PdAu-5K-100AA	11.6	0	90
PdAu-10K-100AA	28.4	0	100

As in the case for the KOAc-only treated samples, no Au was detected in the filtrate of the AcOH-treated and AcOH/KOAc-treated samples, indicating no Au leaching. We were also able to achieve >90% recovery of K for all samples containing K, confirming initial loadings of either 5 wt% or 10 wt% K. The sample without KOAc showed 7.4% Pd loss in the filtrate, indicating treatment in AcOH alone is able to leach noticeable amounts of Pd. However, mixing KOAc with AcOH in the wet impregnation solution caused Pd loss in the filtrate to increase approximately

ten-fold from 1.7 to 11.6% and 2.1 to 28.4% for the 5 wt% and 10 wt% added K, respectively. The Pd loss comes from leaching of these Pd-acetate species, further confirmed by the lack of acetate peaks in the DRIFTS spectra of the washed samples (Figure S3b) as well as the presence of brown-colored particles suspended in the collected filtrate (Figure S4).

3.5 XAS Analysis of PdAu/SiO_2 Treated in KOAc, AcOH, and AcOH/KOAc Solutions

X-ray absorption spectroscopy (XAS) was conducted at the Au L_{III} and Pd K edges. The XANES energy of the Au L_{III} edge, defined here at the only inflection point of the initial photoexcitation, is lower for all of the samples compared to the Au foil, indicating the formation of Pd-Au bonds (Figure 7, Table S1).

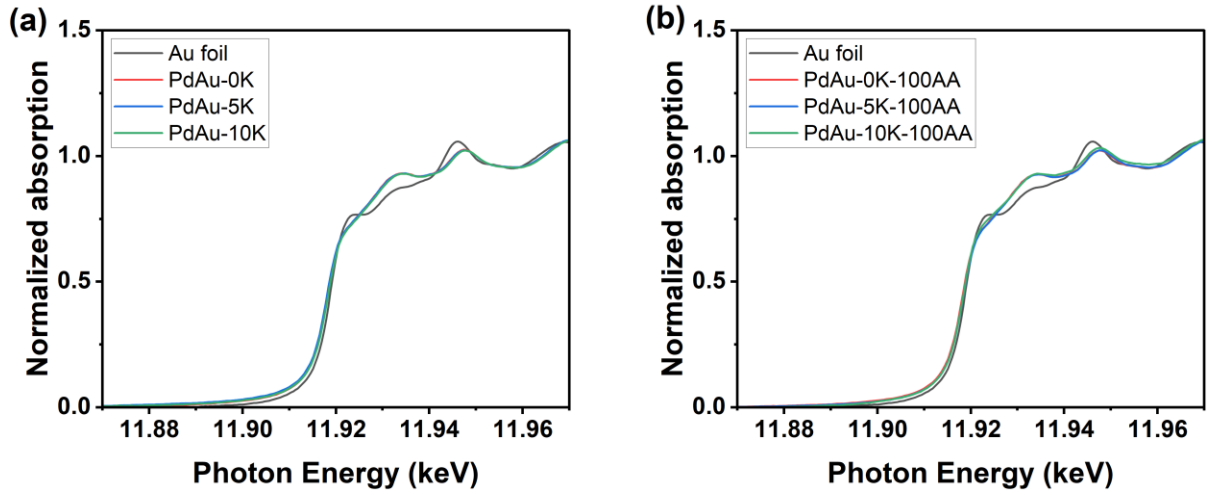

Figure 7. Au L_{III} edge XANES for the Au foil (black) and KOAc-impregnated PdAu/SiO_2 samples containing 0 (red), 5 (blue), and 10 (green) wt% K treated in either (a) water or (b) AcOH solution.

Figure 7 shows that all samples are identical from the Au L_{III} edge regardless of treatment. EXAFS fitting shows the existence of both Au-Au and Au-Pd scattering paths with no evidence of a Au-O scattering path, indicating the Au is completely metallic (Table S1). In a perfect Pd_3Au intermetallic phase, no Au-Au bonds are expected to form. However, the fitting results illustrate that there are approximately 5 Au-Au bonds for every 6 Au-Pd bonds, supporting the XRD data which shows both a ~$Pd_{75}Au_{25}$ alloy phase and pure Au phase for all samples.

At the Pd K edge, the XANES of the PdAu/SiO_2 samples treated with KOAc/water solutions (Figure S5a) shows no change compared to the Pd foil whereas samples treated in KOAc/AcOH solutions (Figure S5b) show a flattening of the XANES profile, indicating formation

of Pd-O bonds. The EXAFS in Figure 8 shows the formation of an alloy with peaks at 2.1 Å and 2.6 Å in *R*. For some samples, a Pd-O peak forms at lower *R*. Upon fitting the EXAFS spectra (Table S2), the as-synthesized sample has a Pd-Pd to Pd-Au coordination number ratio of approximately 3:1. Since a pure Pd_3Au intermetallic phase has a Pd-Pd to Pd-Au coordination number ratio of 2:1, the as-synthesized $PdAu/SiO_2$ must either be a PdAu alloy with a Pd:Au atomic ratio greater than 3:1 or a Pd_3Au alloy containing a separate Pd-only phase. This is consistent with the XRD results showing a pure Au phase, $Pd_{75}Au_{25}$ alloy phase, and a significant amount of XRD-invisible Pd (~45%).

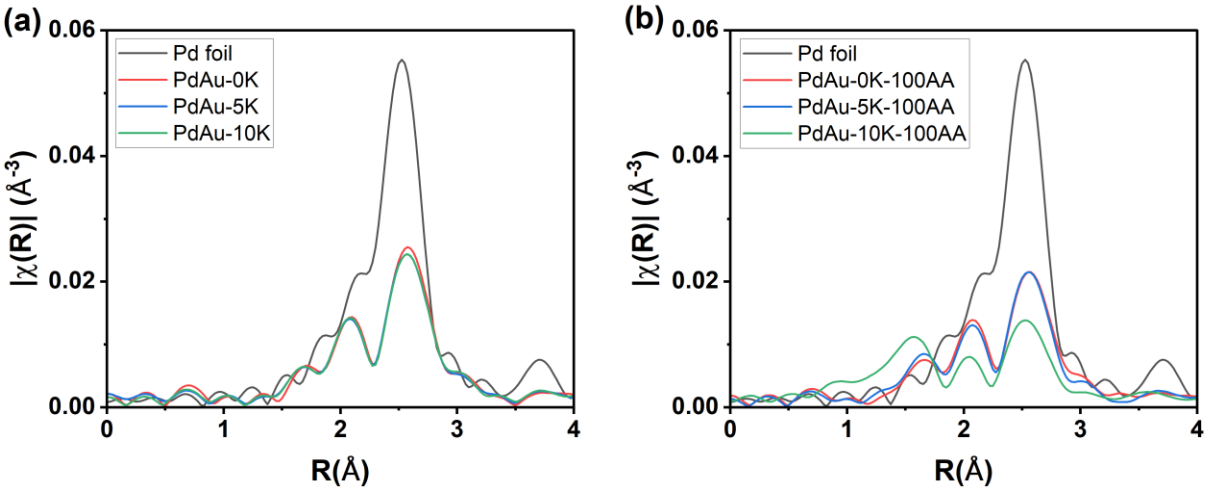

Figure 8. Pd K edge EXAFS for the Pd foil (black) and KOAc-impregnated $PdAu/SiO_2$ samples containing 0 (red), 5 (blue), and 10 (green) wt% K treated in either (a) water or (b) AcOH solution.

The samples that were treated with KOAc/water solutions (Figure 8a, Table S2) remain metallic, as there is no evidence of Pd-O bonds, and were identical to the as-synthesized $PdAu/SiO_2$ sample. The samples treated with KOAc/AcOH solutions (Figure 8b, Table S2) reveal partial oxidation of the Pd, indicated by the decrease in the metallic peaks at 2.6 Å in *R* and the growth of an oxide peak at less than 2 Å in *R*. Additionally, the sample treated with 10 wt % K in AcOH solution (PdAu-10K-100AA) contained the highest degree of Pd oxidation (Figure 8b, Table S2). In this sample, over half of the Pd atoms are oxidized at room temperature under ambient gas conditions as estimated from the Pd-O coordination number as a fraction of total possible Pd-O coordination in a bulk oxide structure (*i.e.* Pd-O *CN* = 4). Interestingly, this differs significantly from the XPS results (Figures 2 and 5) which suggests only metallic Pd is present on

all the samples. However, Pd-acetate species are known to volatilize under UHV conditions,[59] indicating they may not be detectible when performing an XPS analysis at standard UHV conditions. The absence of any bulk PdO peaks in both XPS and XRD data provides further evidence that any Pd-O coordination detected by XAS is associated with Pd-acetate formation.

3.6 Multivariate Analysis

To better understand the changes induced by the wet impregnation of KOAc and/or AcOH, we employed a Design of Experiments (DOE) approach to identify statistically significant trends and relationships regarding metal structure and surface species as functions of K wt% and AcOH vol%. In order to complete the 3^2 full factorial experimental design presented in Table 1, additional samples were prepared by impregnating the as-synthesized PdAu/SiO_2 with KOAc in a solution of 50 vol% AcOH (v/v in water) to achieve KOAc loadings of 0, 5, or 10 wt% K (herein labeled "PdAu-0K-50AA", "PdAu-5K-50AA", and "PdAu-10K-50AA", respectively). Triplicates of the PdAu-5K-50AA sample were prepared to represent the level-(0,0) center point. XRD, XPS, DRIFTS, XAS, and ICP-OES data were collected and analyzed for these samples (Figures S6-S9, Tables S1-S4), and had similar structures and surface species as the previous samples.

Figure 9 shows the response surfaces for Au and Pd_xAu_y alloy grain size determined from XRD data. There is a clear trend that higher AcOH concentration in the wet impregnation solution leads to larger grain sizes in both the Au and Pd_xAu_y nano-domains. Analysis of the response surfaces reveals that effects from AcOH vol% are indeed statistically significant for changes in both Au and Pd_xAu_y grain sizes (Figure S10 and S11). Interestingly, the addition of KOAc to impregnation solutions containing high AcOH concentrations diminished the enlargement effect on Au grain size, indicating interactions between AcOH and KOAc could be a major contributor to the Au grain size response (Figure S10), which is likely due to pH neutralization when KOAc is added to AcOH.

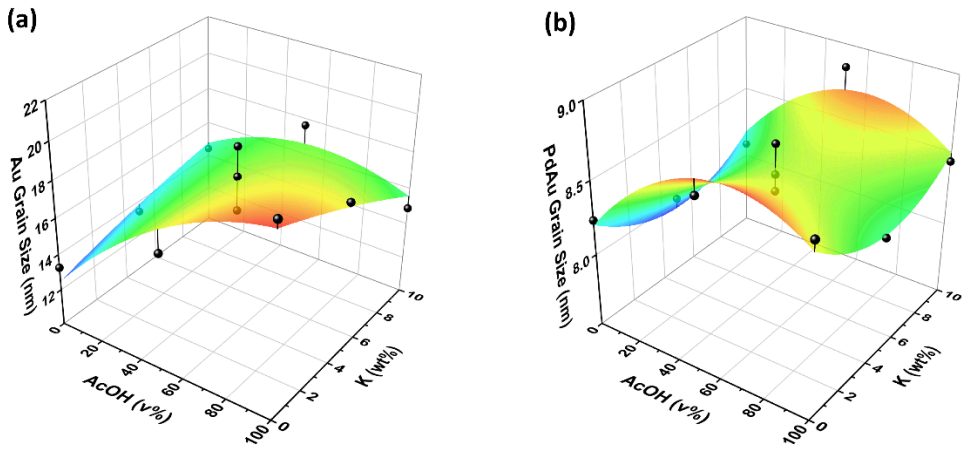

Figure 9. Response surfaces for (a) Au grain size (R^2 = 0.82) and (b) PdAu grain size (R^2 = 0.85) determined from XRD versus K wt% and AcOH vol%.

Figure 10a shows the response surface for Pd surface content determined from XPS data. It is evident that increasing both AcOH and KOAc concentrations in the wet impregnation solutions reduces Pd content on the nanoparticle surface, likely due to the leaching of oxidized Pd species. The response surface for total Pd^{2+} content determined from XAS data (Figure 10b) strongly supports this finding since a significant percent of Pd^{2+} is present after wet impregnation when high concentrations of AcOH and KOAc are used. The response surfaces for monodentate acetate adsorbed on surface Pd (Figure 10c), $Pd_3(OAc)_6$ trimer (Figure 10d), and $K_2Pd_2(OAc)_6$ dimer (Figure 10e) show a strong positive correlation with the Pd^{2+} response surface. The response curve for Pd loss detected by ICP-OES (Figure 10f) also shows a strong positive correlation with these Pd-acetate species.

Collectively, the response surfaces in Figure 10 reveal that a considerable amount of Pd leached from the washed catalysts, as various Pd-acetate species formed during impregnation with KOAc in AcOH solutions. Pareto charts of the standardized effects for all the responses (Figures S12-S17) confirm that the effects from both factors (AcOH vol% and KOAc wt%) and their interactions are statistically significant.

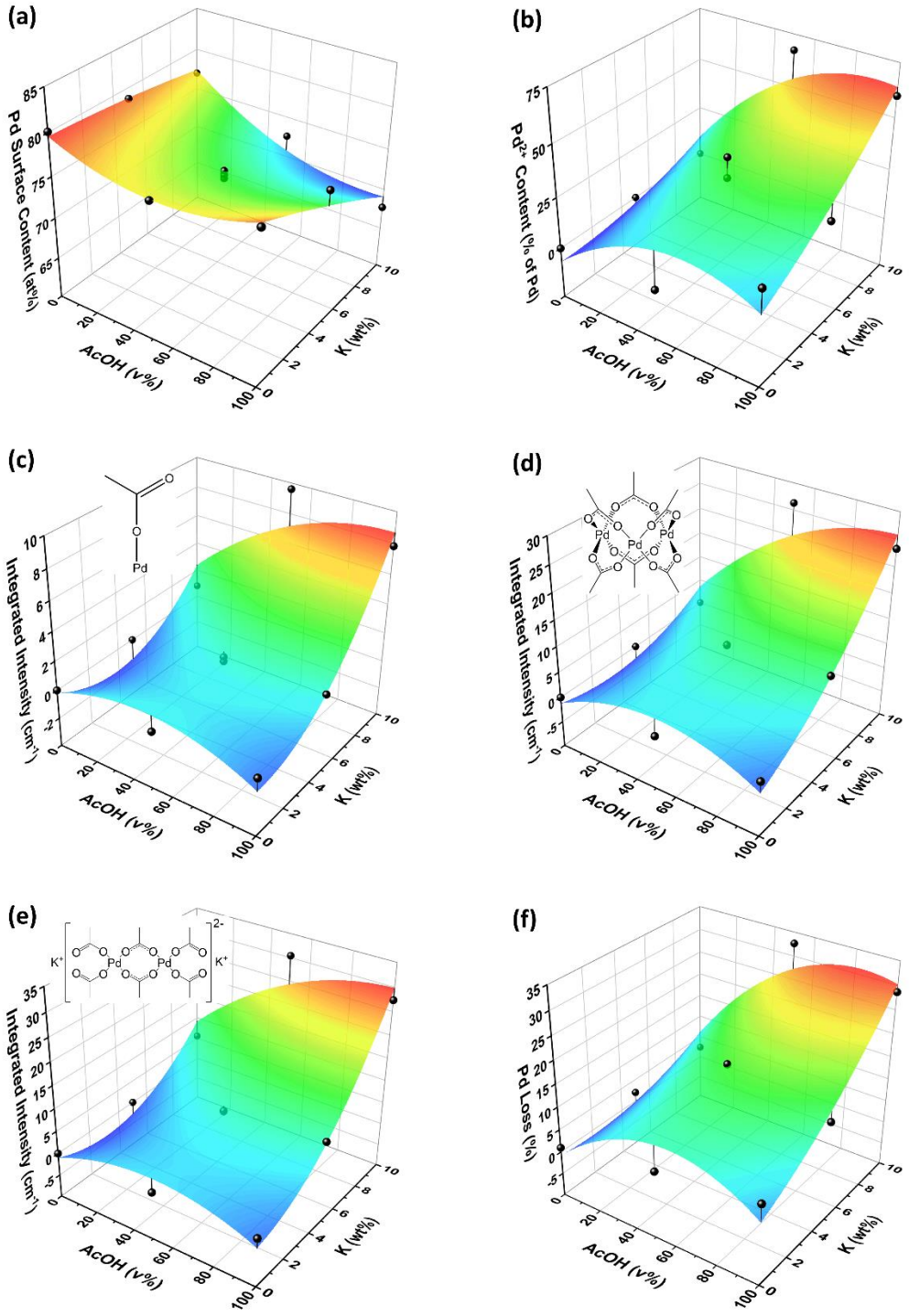

Figure 10. Response surfaces for (a) Pd surface content (R^2 = 0.92) determined from XPS, (b) Pd^{2+} content as percent of total Pd (R^2 = 0.83) determined from Pd-O *CN* at Pd K edge, (c) monodentate acetate adsorbed on surface Pd (R^2 = 0.88), (d) $Pd_3(OAc)_6$ trimer (R^2 = 0.93), (e) $K_2Pd_2(OAc)_6$ dimer (R^2 = 0.91) reported as DRIFTS integrated intensities, and (f) Pd loss in filtrate (R^2 = 0.91) versus K wt% and AcOH vol%.

3.7 Implications for VAM Catalysis

Early characterizations by Nakamura and Yasui first reported the presence of leached Pd-acetate on Pd catalysts after exposure to VAM reaction conditions.[60,61] The existence of this species during the VAM reaction was later confirmed by Augustine and Blitz using *in situ* DRIFTS characterization.[62] It has been proposed that the loss of Pd as leached Pd-acetate species occurs due to the adsorption of an AcOH multilayer film on the catalyst surface,[6] ultimately leading to catalyst deactivation.[63] However, Kragten et al. reported that Pd-acetate in the presence of KOAc exists as dimeric $K_2Pd_2(OAc)_6$ and is catalytically active for the liquid-phase VAM reaction.[5] Lercher and coworkers later identified this dimeric $K_2Pd_2(OAc)_6$ and corresponding PdAu nanoparticle restructuring via *in situ* characterizations during the gas-phase VAM reaction.[9]

Our findings suggest a similar pathway for metal loss and restructuring of $PdAu/SiO_2$ catalysts simply during the wet impregnation of KOAc in presence of AcOH. Spectroscopic characterization of these samples revealed substantial quantities of leached trimeric $Pd_3(OAc)_6$, which would presumably lead to decreased catalyst activity due to Pd loss.[63] However, catalytically active $K_2Pd_2(OAc)_6$ dimer[5] was also present on the same samples. Furthermore, we identified by DRIFTS acetate adsorbed on surface Pd in a monodentate mode, which participates in the surface reaction mechanism by coupling with ethylene adsorbed on a neighboring Pd site followed by β-hydride elimination to form VAM.[64–66] Although it is currently unclear whether these combined contributions will increase catalyst activity or cause deactivation, we nevertheless show that standard catalyst preparation procedures have the potential to drastically alter the catalyst structure and composition even before exposure to VAM reaction conditions.

4. Conclusions

In this work, a $PdAu/SiO_2$ model catalyst was successfully synthesized containing pure Au and Pd-rich PdAu phases. This catalyst was impregnated with varying loadings of KOAc (0, 5, and 10 wt% K) using wet impregnation with varying concentrations of AcOH (0, 50, and 100 vol% AcOH in water). Samples were characterized to detect changes in metal nanoparticle structure (XRD, XPS, and XAS) and surface species formation (DRIFTS). XRD-detectable compositions remained unchanged after all impregnation treatments. Impregnation using solutions containing KOAc without AcOH formed $Pd_3(OAc)_6$ trimers, while no XRD-detectible changes were observed.

Impregnation of only glacial AcOH caused significant enlargement of Au grain size and minimal Pd-acetate formation detected by DRIFTS. However, addition of KOAc to the AcOH solution caused substantial leaching of Pd from the nanoparticle surface as $K_2Pd_2(OAc)_6$ and $Pd_3(OAc)_6$, leading to up to 32% Pd loss after washing with water. Multivariate analysis confirmed the effects from KOAc and AcOH were statistically significant. Ultimately, these findings suggest care should be taken during the wet impregnation process of salt promoters as we demonstrate that metal leaching and structural modifications can occur.

Author Contributions

H. P. Jacobs: conceptualization, formal analysis, investigation, visualization, writing – original draft. W. C. Elias: conceptualization, formal analysis, investigation, visualization, writing – review & editing. K. N. Heck: conceptualization, supervision, writing – review & editing. D. P. Dean: investigation, visualization, writing – review & editing. J. J. Dodson: supervision, writing – review & editing. W. Zhang: conceptualization, investigation, validation. J. H. Arredondo: supervision, methodology. C. J. Breckner, K. Hong, and C. R. Botello: investigation, validation. L. Chen, S. G. Mueller, and S. R. Alexander: supervision, writing – review & editing. J. T. Miller: resources, supervision, writing – review & editing. M. S. Wong: conceptualization, funding acquisition, project administration, supervision, writing – review & editing.

Conflicts of Interest

There are no conflicts to declare.

Acknowledgements

The authors gratefully acknowledge support from Celanese Corporation and ACS-PRF Grant #61790-ND5. The authors thank the Rice University Shared Equipment Authority (SEA) for use of the XPS and ICP-OES equipment. MRCAT operations are supported by the Department of Energy and the MRCAT member institutions. This research used resources of the Advanced Photon Source, a U.S. Department of Energy (DOE) Office of Science User Facility operated for the DOE Office of Science by Argonne National Laboratory under Contract No. DE-AC02-06CH11357.

REFERENCES

(1) Ben Halima, N. Poly(Vinyl Alcohol): Review of Its Promising Applications and Insights into Biodegradation. *RSC Adv.* **2016**, *6* (46), 39823–39832. https://doi.org/10.1039/C6RA05742J.

(2) Speetjens, F. W.; Mahanthappa, M. K. Synthesis and Rheological Characterization of Poly(Vinyl Acetate- *b* -Vinyl Alcohol- *b* -Vinyl Acetate) Triblock Copolymer Hydrogels. *Macromolecules* **2015**, *48* (15), 5412–5422. https://doi.org/10.1021/acs.macromol.5b00410.

(3) Smidt, J.; Hafner, W.; Jira, R.; Sieber, R.; Sedlmeier, J.; Sabel, A. The Oxidation of Olefins with Palladium Chloride Catalysts. *Angew. Chem. Int. Ed. Engl.* **1962**, *1* (2), 80–88. https://doi.org/10.1002/anie.196200801.

(4) Grover, G. S.; Chaudhari, R. V. Kinetics of Oxidation of Ethylene to Vinyl Acetate Using a Homogeneous Palladium Complex Catalyst. *Chem. Eng. J.* **1986**, *32* (2), 93–99. https://doi.org/10.1016/0300-9467(86)80056-9.

(5) Kragten, D. D.; R. A. Santen, V.; Crawford, M. K.; Provine, W. D.; Lerou, J. J. A Spectroscopic Study of the Homogenous Catalytic Conversion of Ethylene to Vinyl Acetate by Palladium Acetate. *Inorg. Chem.* **1999**, *38* (2), 331–339. https://doi.org/10.1021/ic980399g.

(6) Crathorne, E. A.; Macgowan, D.; Morris, S. R.; Rawlinson, A. P. Application of Isotopic Transient Kinetics to Vinyl Acetate Catalysis. *J. Catal.* **1994**, *149* (2), 254–267. https://doi.org/10.1006/jcat.1994.1294.

(7) Voskanyan, P. S. Effect of the Amounts and Proportions of Active Components on the Activity and Selectivity of a Catalyst for Vinyl Acetate Synthesis by Gas-Phase Ethylene Acetoxylation. *Catal. Ind.* **2010**, *2* (2), 167–172. https://doi.org/10.1134/S2070050410020121.

(8) Provine, W. D.; Mills, P. L.; Lerou, J. J. Discovering the Role of Au and KOAc in the Catalysis of Vinyl Acetate Synthesis. In *Studies in Surface Science and Catalysis*; Hightower, J. W., Nicholas Delgass, W., Iglesia, E., Bell, A. T., Eds.; 11th International Congress On Catalysis - 40th Anniversary; Elsevier, 1996; Vol. 101, pp 191–200. https://doi.org/10.1016/S0167-2991(96)80229-1.

(9) Hanrieder, E. K.; Jentys, A.; Lercher, J. A. Atomistic Engineering of Catalyst Precursors: Dynamic Reordering of PdAu Nanoparticles during Vinyl Acetate Synthesis Enhanced by Potassium Acetate. *ACS Catal.* **2015**, *5* (10), 5776–5786. https://doi.org/10.1021/acscatal.5b01140.

(10) Hanrieder, E. K.; Jentys, A.; Lercher, J. A. Impact of Alkali Acetate Promoters on the Dynamic Ordering of PdAu Catalysts during Vinyl Acetate Synthesis. *J. Catal.* **2016**, *333*, 71–77. https://doi.org/10.1016/j.jcat.2015.10.019.

(11) Hanrieder, E. K.; Jentys, A.; Lercher, J. A. Interaction of Alkali Acetates with Silica Supported PdAu. *Catal. Sci. Technol.* **2016**, *6* (19), 7203–7211. https://doi.org/10.1039/C6CY01228K.

(12) Ertl, G.; Knozinger, H.; Weitkamp, J. *Handbook of Heterogeneous Catalysis*, 2nd ed.; Wiley-VCH: Weinheim, Germany, 1997.

(13) Nakaya, Y.; Hayashida, E.; Shi, R.; Shimizu, K.; Furukawa, S. Interstitial Carbon Dopant in Palladium–Gold Alloy Boosting the Catalytic Performance in Vinyl Acetate Monomer Synthesis. *J. Am. Chem. Soc.* **2023**, *145* (5), 2985–2998. https://doi.org/10.1021/jacs.2c11481.

(14) Yin, Y. B.; Heck, K. N.; Coonrod, C. L.; Powell, C. D.; Guo, S.; Reynolds, M. A.; Wong, M. S. PdAu-Catalyzed Oxidation through in Situ Generated H2O2 in Simulated Produced Water. *Catal. Today* **2020**, *339*, 362–370. https://doi.org/10.1016/j.cattod.2019.05.001.

(15) Edwards, J. K.; Solsona, B. E.; Landon, P.; Carley, A. F.; Herzing, A.; Kiely, C. J.; Hutchings, G. J. Direct Synthesis of Hydrogen Peroxide from H2 and O2 Using TiO2-Supported Au–Pd Catalysts. *J. Catal.* **2005**, *236* (1), 69–79. https://doi.org/10.1016/j.jcat.2005.09.015.

(16) Ricciardulli, T.; Gorthy, S.; Adams, J. S.; Thompson, C.; Karim, A. M.; Neurock, M.; Flaherty, D. W. Effect of Pd Coordination and Isolation on the Catalytic Reduction of O2 to H2O2 over PdAu Bimetallic Nanoparticles. *J. Am. Chem. Soc.* **2021**, *143* (14), 5445–5464. https://doi.org/10.1021/jacs.1c00539.

(17) Zhao, Z.; Miller, J. T.; Wu, T.; Schweitzer, N. M.; Wong, M. S. EXAFS Characterization of Palladium-on-Gold Catalysts Before and After Glycerol Oxidation. *Top. Catal.* **2015**, *58* (4), 302–313. https://doi.org/10.1007/s11244-015-0371-3.

(18) Zhao, Z.; Arentz, J.; Pretzer, L. A.; Limpornpipat, P.; Clomburg, J. M.; Gonzalez, R.; Schweitzer, N. M.; Wu, T.; Miller, J. T.; Wong, M. S. Volcano-Shape Glycerol Oxidation Activity of Palladium-Decorated Gold Nanoparticles. *Chem. Sci.* **2014**, *5* (10), 3715–3728. https://doi.org/10.1039/C4SC01001A.

(19) Nutt, M. O.; Hughes, J. B.; Wong, M. S. Designing Pd-on-Au Bimetallic Nanoparticle Catalysts for Trichloroethene Hydrodechlorination. *Environ. Sci. Technol.* **2005**, *39* (5), 1346–1353. https://doi.org/10.1021/es048560b.

(20) Qian, H.; Zhao, Z.; Velazquez, J. C.; Pretzer, L. A.; Heck, K. N.; Wong, M. S. Supporting Palladium Metal on Gold Nanoparticles Improves Its Catalysis for Nitrite Reduction. *Nanoscale* **2013**, *6* (1), 358–364. https://doi.org/10.1039/C3NR04540D.

(21) Liu, P.; Nørskov, J. K. Ligand and Ensemble Effects in Adsorption on Alloy Surfaces. *Phys. Chem. Chem. Phys.* **2001**, *3* (17), 3814–3818. https://doi.org/10.1039/B103525H.

(22) Yi, C.-W.; Luo, K.; Wei, T.; Goodman, D. W. The Composition and Structure of Pd−Au Surfaces. *J. Phys. Chem. B* **2005**, *109* (39), 18535–18540. https://doi.org/10.1021/jp053515r.

(23) Zhang, M.; Hao, Q.; Yu, Y. Pd/Au(100) Alloy for Vinyl Acetate Synthesis: Effects of Surface Properties on Reagents Adsorption. *Comput. Theor. Chem.* **2013**, *1019*, 33–38. https://doi.org/10.1016/j.comptc.2013.06.001.

(24) Kumar, D.; Chen, M. S.; Goodman, D. W. Synthesis of Vinyl Acetate on Pd-Based Catalysts. *Catal. Today* **2007**, *123* (1–4), 77–85. https://doi.org/10.1016/j.cattod.2007.01.050.

(25) Chen, M. S.; Luo, K.; Wei, T.; Yan, Z.; Kumar, D.; Yi, C.-W.; Goodman, D. W. The Nature of the Active Site for Vinyl Acetate Synthesis over Pd–Au. *Catal. Today* **2006**, *117* (1), 37–45. https://doi.org/10.1016/j.cattod.2006.05.001.

(26) Chen, M.; Kumar, D.; Yi, C.-W.; Goodman, D. W. The Promotional Effect of Gold in Catalysis by Palladium-Gold. *Science* **2005**, *310* (5746), 291–293. https://doi.org/10.1126/science.1115800.

(27) Gravelle-Rumeau-Maillot, M.; Pitchon, V.; Martin, G. A.; Praliaud, H. Complementary Study by Calorimetry and Infrared Spectroscopy of Alkali Metal Doped Pd/SiO2 Solids: Adsorption of Hydrogen and Carbon Monoxide. *Appl. Catal. Gen.* **1993**, *98* (1), 45–59. https://doi.org/10.1016/0926-860X(93)85024-J.

(28) Pitchon, V.; Guenin, M.; Praliaud*, H. X-Ray Photoelectron Spectroscopic Study of the Electronic State of Palladium in Alkali Metal Doped Pd/SiO2 Solids. *Appl. Catal.* **1990**, *63* (1), 333–343. https://doi.org/10.1016/S0166-9834(00)81723-6.

(29) Vinyl Acetate Monomer Process. In *Chemical Process Design*; John Wiley & Sons, Ltd, 2008; pp 287–312. https://doi.org/10.1002/9783527621583.ch10.

(30) Davidson, A. W.; McAllister, W. H. SOLUTIONS OF SALTS IN PURE ACETIC ACID. II. SOLUBILITIES OF ACETATES1. *J. Am. Chem. Soc.* **1930**, *52* (2), 507–519. https://doi.org/10.1021/ja01365a010.

(31) Samanos, B.; Boutry, P.; Montarnal, R. The Mechanism of Vinyl Acetate Formation by Gas-Phase Catalytic Ethylene Acetoxidation. *J. Catal.* **1971**, *23* (1), 19–30. https://doi.org/10.1016/0021-9517(71)90019-4.

(32) Reilly, C. R.; Lerou, J. J. Supported Liquid Phase Catalysis in Selective Oxidation. *Catal. Today* **1998**, *41* (4), 433–441. https://doi.org/10.1016/S0920-5861(98)00029-7.

(33) Stoyanov, E. S. Ir Study of the Structure of Palladium(Ii) Acetate in Chloroform, Acetic Acid, and Their Mixtures in Solution and in Liquid-Solid Subsurface Layers. *J. Struct. Chem.* **2000**, *41* (3), 440–445. https://doi.org/10.1007/BF02742003.

(34) Pandey, R. N.; Henry, P. M. Interaction of Palladium(II) Acetate with Sodium and Lithium Acetate in Acetic Acid. *Can. J. Chem.* **1974**, *52* (8), 1241–1247. https://doi.org/10.1139/v74-193.

(35) Pandey, R. N.; Henry, P. M. Equilibria between Palladium(II) Acetate and Olefins in Acetic Acid Containing Sodium Acetate. *Can. J. Chem.* **1975**, *53* (12), 1833–1841. https://doi.org/10.1139/v75-255.

(36) Simson, S.; Jentys, A.; Lercher, J. A. Dynamic Self-Organization of Supported Pd/Au Catalysts during Vinyl Acetate Synthesis. *J. Phys. Chem. C* **2013**, *117* (16), 8161–8169. https://doi.org/10.1021/jp3119764.

(37) Vegard, L. Die Konstitution der Mischkristalle und die Raumfüllung der Atome. *Z. Für Phys.* **1921**, *5* (1), 17–26. https://doi.org/10.1007/BF01349680.

(38) Scherrer, P. Bestimmung der inneren Struktur und der Größe von Kolloidteilchen mittels Röntgenstrahlen. In *Kolloidchemie Ein Lehrbuch*; Zsigmondy, R., Ed.; Chemische Technologie in Einzeldarstellungen; Springer: Berlin, Heidelberg, 1912; pp 387–409. https://doi.org/10.1007/978-3-662-33915-2_7.

(39) Wagner, C. D.; Passoja, D. E.; Hillery, H. F.; Kinisky, T. G.; Six, H. A.; Jansen, W. T.; Taylor, J. A. Auger and Photoelectron Line Energy Relationships in Aluminum–Oxygen and

718 Silicon–Oxygen Compounds. *J. Vac. Sci. Technol.* **1982**, *21* (4), 933–944.
719 https://doi.org/10.1116/1.571870.

720 (40) Segre, C. U.; Leyarovska, N. E.; Chapman, L. D.; Lavender, W. M.; Plag, P. W.; King, A.
721 S.; Kropf, A. J.; Bunker, B. A.; Kemner, K. M.; Dutta, P.; Duran, R. S.; Kaduk, J. The
722 MRCAT Insertion Device Beamline at the Advanced Photon Source. *AIP Conf. Proc.* **2000**,
723 *521* (1), 419–422. https://doi.org/10.1063/1.1291825.

724 (41) Ressler, T. WinXAS: A Program for X-Ray Absorption Spectroscopy Data Analysis under
725 MS-Windows. *J. Synchrotron Radiat.* **1998**, *5* (2), 118–122.
726 https://doi.org/10.1107/S0909049597019298.

727 (42) Rehr, J. J.; Booth, C. H.; Bridges, F.; Zabinsky, S. I. X-Ray-Absorption Fine Structure in
728 Embedded Atoms. *Phys. Rev. B* **1994**, *49* (17), 12347–12350.
729 https://doi.org/10.1103/PhysRevB.49.12347.

730 (43) Owen, E. A.; Yates, E. L. XLI. Precision Measurements of Crystal Parameters. *Lond. Edinb.*
731 *Dublin Philos. Mag. J. Sci.* **1933**, *15* (98), 472–488.
732 https://doi.org/10.1080/14786443309462199.

733 (44) Spreadborough, J.; Christian, J. W. High-Temperature X-Ray Diffractometer. *J. Sci. Instrum.*
734 **1959**, *36* (3), 116–118. https://doi.org/10.1088/0950-7671/36/3/302.

735 (45) Lee, Y.-S.; Jeon, Y.; Chung, Y.-D.; Lim, K.-Y.; Whang, C.-N.; Oh, S.-J. Charge
736 Redistribution and Electronic Behavior in Pd-Au Alloys. *J. Korean Phys. Soc.* **2000**, *37* (4),
737 451.

738 (46) X-Ray Photoelectron Spectroscopy Database XPS,Version 4.1, NIST Standard Reference
739 Database 20, 2000. https://doi.org/10.18434/T4T88K.

740 (47) Ertl, G.; Lee, S. B.; Weiss, M. The Influence of Potassium on the Adsorption of Hydrogen
741 on Iron. *Surf. Sci. Lett.* **1981**, *111* (2), L711–L715. https://doi.org/10.1016/0167-
742 2584(81)90666-6.

743 (48) Koukiou, S.; Konsolakis, M.; Lambert, R. M.; Yentekakis, I. V. Spectroscopic Evidence for
744 the Mode of Action of Alkali Promoters in Pt-Catalyzed de-NOx Chemistry. *Appl. Catal. B*
745 *Environ.* **2007**, *76* (1), 101–106. https://doi.org/10.1016/j.apcatb.2007.05.014.

746 (49) Hayden, B. E.; Robinson, A. W.; Tucker, P. M. An Infra-Red Study of CO Adsorption on
747 Potassium-Doped Pt(110)-(1 × 2); the Long Range Potassium-CO Interaction. *J. Electron*
748 *Spectrosc. Relat. Phenom.* **1987**, *44* (1), 297–304. https://doi.org/10.1016/0368-
749 2048(87)87030-5.

750 (50) Tom, H. W. K.; Mate, C. M.; Zhu, X. D.; Crowell, J. E.; Shen, Y. R.; Somorjai, G. A. Studies
751 of Alkali Adsorption on Rh(111) Using Optical Second-Harmonic Generation. *Surf. Sci.*
752 **1986**, *172* (2), 466–476. https://doi.org/10.1016/0039-6028(86)90768-5.

753 (51) Brijaldo, M. H.; Rojas, H. A.; Martínez, J. J.; Passos, F. B. Effect of Support on Acetic Acid
754 Decomposition over Palladium Catalysts. *J. Catal.* **2015**, *331*, 63–75.
755 https://doi.org/10.1016/j.jcat.2015.08.019.

756 (52) Green, I. X.; Tang, W.; Neurock, M.; Yates, J. T. Mechanistic Insights into the Partial
757 Oxidation of Acetic Acid by O2 at the Dual Perimeter Sites of a Au/TiO2 Catalyst. *Faraday*
758 *Discuss.* **2013**, *162* (0), 247–265. https://doi.org/10.1039/C3FD00002H.

(53) McDonald, R. S. Surface Functionality of Amorphous Silica by Infrared Spectroscopy. *J. Phys. Chem.* **1958**, *62* (10), 1168–1178. https://doi.org/10.1021/j150568a004.

(54) Rivalta, I.; Mazzone, G.; Russo, N.; Sicilia, E. Adsorption of Ethylene, Vinyl, Acetic Acid, and Acetate Species on PdAu(111) and PdAu(100) Surface Alloys: A Cluster Model Study. *J. Chem. Theory Comput.* **2009**, *5* (5), 1350–1360. https://doi.org/10.1021/ct9000137.

(55) Sirita, J.; Phanichphant, S.; Meunier, F. C. Quantitative Analysis of Adsorbate Concentrations by Diffuse Reflectance FT-IR. *Anal. Chem.* **2007**, *79* (10), 3912–3918. https://doi.org/10.1021/ac0702802.

(56) Behravesh, E.; Kumar, N.; Balme, Q.; Roine, J.; Salonen, J.; Schukarev, A.; Mikkola, J.-P.; Peurla, M.; Aho, A.; Eränen, K.; Murzin, D. Yu.; Salmi, T. Synthesis and Characterization of Au Nano Particles Supported Catalysts for Partial Oxidation of Ethanol: Influence of Solution PH, Au Nanoparticle Size, Support Structure and Acidity. *J. Catal.* **2017**, *353*, 223–238. https://doi.org/10.1016/j.jcat.2017.07.014.

(57) Patungwasa, W.; Hodak, J. H. PH Tunable Morphology of the Gold Nanoparticles Produced by Citrate Reduction. *Mater. Chem. Phys.* **2008**, *108* (1), 45–54. https://doi.org/10.1016/j.matchemphys.2007.09.001.

(58) Wolf, A.; Schüth, F. A Systematic Study of the Synthesis Conditions for the Preparation of Highly Active Gold Catalysts. *Appl. Catal. Gen.* **2002**, *226* (1), 1–13. https://doi.org/10.1016/S0926-860X(01)00772-4.

(59) Gallagher, P. K.; Gross, M. E. The Thermal Decomposition of Palladium Acetate. *J. Therm. Anal.* **1986**, *31* (6), 1231–1241. https://doi.org/10.1007/BF01914636.

(60) Nakamura, S.; Yasui, T. The Mechanism of the Palladium-Catalyzed Synthesis of Vinyl Acetate from Ethylene in a Heterogeneous Gas Reaction. *J. Catal.* **1970**, *17* (3), 366–374. https://doi.org/10.1016/0021-9517(70)90113-2.

(61) Nakamura, S.; Yasui, T. Formation of Palladous Acetate and Stability of Catalyst in Palladium-Metal-Catalyzed Synthesis of Vinyl Acetate from Ethylene. *J. Catal.* **1971**, *23* (3), 315–320. https://doi.org/10.1016/0021-9517(71)90220-X.

(62) Augustine, S. M.; Blitz, J. P. The Use of DRIFTS-MS and Kinetic Studies to Determine the Role of Acetic Acid in the Palladium-Catalyzed Vapor-Phase Synthesis of Vinyl Acetate. *J. Catal.* **1993**, *142* (1), 312–324. https://doi.org/10.1006/jcat.1993.1210.

(63) Pohl, M.-M.; Radnik, J.; Schneider, M.; Bentrup, U.; Linke, D.; Brückner, A.; Ferguson, E. Bimetallic PdAu–KOac/SiO2 Catalysts for Vinyl Acetate Monomer (VAM) Synthesis: Insights into Deactivation under Industrial Conditions. *J. Catal.* **2009**, *262* (2), 314–323. https://doi.org/10.1016/j.jcat.2009.01.008.

(64) Calaza, F.; Mahapatra, M.; Neurock, M.; Tysoe, W. T. Disentangling Ensemble, Electronic and Coverage Effects on Alloy Catalysts: Vinyl Acetate Synthesis on Au/Pd(111). *J. Catal.* **2014**, *312*, 37–45. https://doi.org/10.1016/j.jcat.2014.01.003.

(65) Neurock, M.; Tysoe, W. T. Mechanistic Insights in the Catalytic Synthesis of Vinyl Acetate on Palladium and Gold/Palladium Alloy Surfaces. *Top. Catal.* **2013**, *56* (15), 1314–1332. https://doi.org/10.1007/s11244-013-0153-8.

(66) Stacchiola, D.; Calaza, F.; Burkholder, L.; Schwabacher, A. W.; Neurock, M.; Tysoe, W. T. Elucidation of the Reaction Mechanism for the Palladium-Catalyzed Synthesis of Vinyl Acetate. *Angew. Chem. Int. Ed.* **2005**, *44* (29), 4572–4574. https://doi.org/10.1002/anie.200500782.